Biallelic mutation in *NADSYN1* cause multiple organ defects and expand the genotypic spectrum of Congenital NAD Deficiency Disorders

Justin O. Szot[1], Carla Campagnolo[2,14], Ye Cao[3,4,5,6,14], Kavitha R. Iyer[1], Hartmut Cuny[1,7], Thomas Drysdale[8,9,10], Josue A. Flores-Daboub[11], Weimin Bi[3,6], Lauren Westerfield[3], Pengfei Liu[3,6], Tse Ngong Leung[5], Kwong Wai Choy[4,12], Gavin Chapman[1,7,15], Rui Xiao[3,6,15], Victoria M. Siu[2,8,15], Sally L. Dunwoodie[1,7,13] *

[1]Victor Chang Cardiac Research Institute, Darlinghurst, Sydney, NSW 2010, Australia.
[2]Division of Medical Genetics, Department of Pediatrics, University of Western Ontario, London, ON N6A 3K7, Canada.
[3]Department of Molecular and Human Genetics, Baylor College of Medicine, Houston, TX 77030, USA.
[4]Department of Obstetrics and Gynaecology, The Chinese University of Hong Kong, Hong Kong SAR, China.
[5]Obstetrics & Gynaecology Centre, Hong Kong Sanatorium & Hospital, Hong Kong SAR, China.
[6]Baylor Genetics, Houston, TX 77021, USA.
[7]Faculty of Medicine, University of New South Wales, Sydney, NSW 2052, Australia.
[8]Children's Health Research Institute, 800 Commissioners Road East, London, ON N6C 2V5, Canada.
[9]Department of Physiology and Pharmacology, Western University, London, ON N6A 5C1, Canada.
[10]Department of Paediatrics, Western University, 800 Commissioners Road East, London, ON N6A 5W9, Canada.
[11]Division of Medical Genetics, Department of Pediatrics, University of Utah, UT 84112, USA.
[12]The Chinese University of Hong Kong-Baylor College of Medicine Joint Center For Medical Genetics, Hong Kong SAR, China.
[13]Faculty of Science, University of New South Wales, Sydney, NSW 2052, Australia.
[14,15]These authors contributed equally to this work

*Correspondence: s.dunwoodie@victorchang.edu.au

Abstract
Birth defects occur in up to 3% of all live births and are the leading cause of infant death. Here we present five individuals from four unrelated families sharing similar phenotypes with disease-causal biallelic variants in *NADSYN1*, encoding NAD synthetase 1, the final enzyme of the nicotinamide adenine dinucleotide (NAD) *de novo* synthesis pathway. Defects range from the isolated absence of both kidneys to multiple malformations of the vertebrae, heart, limbs, and kidney, with no individual surviving more than three months postnatally. NAD is an essential coenzyme for numerous cellular processes. Biallelic loss-of-function mutations in genes required for the *de novo* synthesis of NAD, were previously identified in individuals with multiple congenital abnormalities affecting the heart, kidney, vertebrae, and limbs. Functional assessments of *NADSYN1* missense variants, through a combination of yeast complementation and enzymatic assays, show impaired enzymatic activity, and severely reduced NAD levels. Thus *NADSYN1* represents an additional gene required for NAD synthesis during embryogenesis with biallelic missense variants causing NAD deficiency-dependent malformations. Our findings expand the genotypic spectrum of Congenital NAD Deficiency Disorders, and further implicate mutation of additional genes involved in *de novo* NAD synthesis as potential causes of complex birth defects.

Keywords
Congenital NAD Deficiency Disorder; NADSYN1; autosomal recessive; kynurenine pathway; NAD; *de novo* NAD synthesis; VACTERL

Main Text
Nicotinamide adenine dinucleotide (NAD) is an essential metabolite functioning as a coenzyme in over 400 cellular redox reactions,[1] with key signaling roles in mitochondrial function and metabolism, DNA repair, cell division, immune response and inflammation, circadian rhythm, protein-protein signaling, and epigenetics.[2] Mammalian cells lack the ability to import NAD, requiring that it be synthesized *de novo* from L-tryptophan via the kynurenine pathway, or from dietary vitamin B3 collectively referring to the NAD precursors nicotinamide, nicotinic acid, and nicotinamide riboside.[2; 3] These precursors can be converted to NAD through the salvage pathway, contributing to the vast majority of the reserve NAD pool in postnatal tissue.[4] Although the relative contribution of *de novo* and salvage pathway to NAD levels is currently unknown during embryogenesis, NAD deficiency caused by *de novo* pathway perturbation during embryogenesis manifests in defective development of the vertebrae, heart, kidney, palate, and limbs.[5] Recessive loss-of-function mutations in two genes encoding sequential enzymes of the *de novo* pathway (*HAAO* [MIM: 617660] and *KYNU* [MIM: 617661]) were identified in individuals with NAD deficiency causing defects of the heart, kidney, and vertebrae. Given the lack of genetic redundancy of *HAAO* and *KYNU*, individuals with *de novo* pathway blockage due to defects in other nonredundant genes might also manifest in NAD deficiency causing Congenital NAD Deficiency Disorder.

Here we report five individuals from four unrelated families identified via GeneMatcher[6] with deleterious biallelic variants in NAD synthetase 1 (*NADSYN1*; HGNC: 29832), a gene encoding the final enzyme of the *de novo* pathway. Individuals presented with multiple overlapping congenital malformations reminiscent

of Congenital NAD Deficiency Disorder (Table 1). In Family 1 (F1), individuals II.1 and II.2 were siblings, born to nonconsanguineous parents (Figure 1). These individuals are homozygous for a missense variant in *NADSYN1* (NM_018161.5) [c.1717G>A p.Ala573Thr], while individual F2.II.1 harbors one copy of this variant and an additional truncating variant [c.1819del p.Val607Trpfs*30]. In Family 3, individual II.4 was the fourth pregnancy, following a healthy 5 year old son, a first trimester miscarriage, and a blighted ovum, and carried two *NADSYN1* missense variants ([c.145T>C p.Cys49Arg]; [c.395G>T p.Trp132Leu]). F4.II.1 carries two truncating variants ([c.735T>A p.Cys245*]; [c.1839C>G p.Tyr613*]). All variants rank >20 by CADD-PHRED,[7] placing them in the top 1% of deleterious variants, and they are predicted pathogenic by PolyPhen-2 HVAR[8] except for p.Cys49Arg (Table 2). All affected residues are highly conserved, as reflected in GERP[9] rejected substitution scores >4, suggestive of intolerance to mutation. Finally, all variants are rare with respect to healthy individuals, and none of them are present in the homozygous state in gnomAD.[10]

All individuals exhibited renal abnormalities (5/5) (Table 1) ranging from a mild hyperechoic renal cortex to the complete absence of both kidneys. The limbs were the next most commonly perturbed (4/5) with individuals exhibiting short proximal long bones or micromelia. Equally common were cardiac (3/5) and vertebral abnormalities (3/5). Vertebral defects included scoliosis with multiple malformed vertebrae and ribs, and segmentation defects of the thoracic, lumbar, and sacral spine, while the heart was either hypoplastic due to underdevelopment of the left ventricle or compromised by malformation of the aorta and pulmonary artery. Extra abnormalities were also apparent (Table 1). Due to the severity of their phenotypes, individuals F3.II.4 and F4.II.1 were terminated at 16 weeks of gestation, while neither individual F1.II.1, F1.II.2, nor F2.II.1 survived more than three months postnatally. Complete phenotypes of *NADSYN1* variant carriers and their respective genetic assessments are presented in the Supplemental Note.

The pathway for the *de novo* synthesis of NAD from tryptophan is largely conserved from bacteria to human. In the case of vertebrate NADSYN1, yeast orthologous protein Qns1 (Qns1p) functions equivalently as the final enzyme in this pathway, converting the precursor nicotinic acid adenine dinucleotide (NaAD) to NAD. Qns1p shares 58% amino acid sequence identity with human NADSYN1 and similarly catalyzes NAD generation through a coupled glutaminase – NAD synthetase fused two-domain system. In addition, the rat homolog of NADSYN1, sharing 86% homology with the human sequence, can rescue function of inactivated Qns1p in yeast.[11] Therefore, we functionally assessed human *NADSYN1* variants via a genetic complementation approach in yeast. *QNS1* is an essential gene in yeast, however, metabolic block as a result of gene inactivation may be overcome through exogenous supplementation of nicotinamide riboside (NR).[12] Therefore, we first generated a haploid yeast line replacing *QNS1* with a geneticin resistance cassette, as previously described,[13] sustained on media supplemented with NR (Supplemental Methods). Δ*qns1* yeast were subsequently transformed with plasmids expressing HA-tagged human wild-type (WT) *NADSYN1*, *NADSYN1 Ala573Thr* mutant, or untagged *HAAO* as a control.

Both WT and mutant enzyme were detected by immunoblot in lysates of Δ*qns1* yeast cultured for 48 hours (Figure 2A and B). Protein was generated by both yeast lines at

equivalent amounts. To next assess the capacity of human NADSYN1 to compensate for loss of Qns1p, Δ*qns1* yeast generating WT NADSYN1 (Δ*qns1* WT) were grown in liquid cultures in the absence of NR for 48 hrs (Figure 2C). Δ*qns1* WT yeast grew equivalently well in the presence or absence of NR (Figure S1), suggesting that human NADSYN1 expression rescues loss of Qns1p as efficiently as bypassing the metabolic block via supplementation with NR. Similar growth to Δ*qns1* WT was seen for Δ*qns1* yeast generating the NADSYN1 p.Ala573Thr (Δ*qns1* p.Ala573Thr) mutant in supplemented conditions (Figure S1). However, in the absence of NR, Δ*qns1* p.Ala573Thr yeast grew at a compromised rate, significantly different to Δ*qns1* WT (Figure 2C). The control Δ*qns1* yeast generating HAAO (Δ*qns1* HAAO) did not grow in the absence of NR supplementation.

To determine if NAD deficiency is the cause of altered growth between Δ*qns1* WT or p.Ala573Thr yeast, we compared total NAD (NAD^+ and NADH)[14] in cell extracts. Δ*qns1* WT, p.Ala573Thr, or HAAO yeast were grown in minimal media supplemented with NR. Yeast were subsequently transferred to media lacking NR, grown, lysed, and NAD concentration determined (Supplemental Methods). Levels of NAD in Δ*qns1* p.Ala573Thr or HAAO yeast were significantly lower than Δ*qns1* WT yeast (Figure 2D), suggesting that reduced growth for yeast generating mutant in non-supplemented conditions was a result of compromised enzymatic activity. Total cellular NAD for Δ*qns1* HAAO yeast was baseline as this protein cannot rescue functionality of yeast Qns1p.

Having shown that mutation of Ala573 in the synthetase domain results in reduced yeast viability as a result of deficient cellular NAD, we questioned if glutaminase mutations also reduced total NAD levels by impaired enzymatic activity. WT NADSYN1, p.Ala573Thr, and p.Trp132Leu mutant protein were found in equivalent levels in in COS-7 cells, while p.Cys49Arg protein levels were significantly reduced (Figure 3A). p.Cys49Arg could not be purified, despite efforts scaling up sample preparation (Figure S3). This decrease in NADSYN1 p.Cys49Arg levels was independent of transfection efficiency (data not shown) and prevented downstream analysis of enzymatic activity. Finally, direct enzymatic assessment of NAD synthetase activity of purified proteins (adapted from Hara et al. [15], Supplemental Methods) revealed that both synthetase mutant (p.Ala573Thr) and glutaminase mutant (p.Trp132Leu) exhibited limited capacity to generate NAD (Figure 3B and C). This confirms that reduced viability of the Δ*qns1* p.Ala573Thr yeast, although sufficient for complementation, was a consequence of impaired NAD synthetase activity.

At a protein level, Ala573 is a highly evolutionarily conserved residue within the P2 loop of the NAD synthetase domain (Figure 4). Crystallographic studies in bacterial NAD synthetase orthologs have revealed that the P2 loop adopts alternating conformations that regulate NaAD accessibility at the active site.[16-19] Within the catalysis state, amino acids corresponding to human Ala573 and Leu575 stabilize the positioning of the bound NaAD. A threonine substitution at Ala573, found in our individual cases, is thus likely to have caused the reduction in NADSYN1 enzymatic activity due to steric hindrance at the active site. This mirrors the 86% reduction of total cellular NAD in Δ*qns1* p.Ala573Thr yeast (Figure 2D), and the corresponding ~342-fold decreased NAD synthetase-specific activity of purified mutant protein (Figure 3B), compared to respective wild-types. It is therefore likely that the

NADSYN1 variant in individuals F1.II.1 and F1.II.2 similarly culminate in reduced NAD levels *in vivo*, below a necessary threshold for normal embryonic development. NAD deficiency is also expected in individuals F2.II.1 and F4.II.1 who exhibit NAD-dependent organ malformations and are either compound heterozygous for the p.Ala573Thr variant and a frameshift ([c.1819del p.Val607Trpfs*30]), or carry two frameshifts ([c.735T>A p.Cys245*]; [c.1839C>G p.Tyr613*]), respectively (Table S1).

Mammalian NADSYN1 represents a catalytically coupled fused-domain system,[20] whereby ammonia produced by glutamine hydrolysis at the glutaminase domain acts as substrate for NaAD amidation. The catalytic linkage between glutaminase and synthetase domains relies on a glutamine-ammonia channel bridging these two domains.[16; 19; 21; 22] This connectedness exists due to multimeric arrangement of NADSYN1 monomers in a ring structure, connected centrally via glutaminase domains with synthetase domains extending outwards.[19; 21] Accordingly, missense mutation of key residues within the glutaminase domain of Qns1p result in compromised synthetase activity incompatible with survival *in vivo*.[21; 22]

It is likely that the phenotype of individual F3.II.4, harboring missense variants in the glutaminase domain (p.Cys49Arg, p.Trp132Leu; Figure 4), is a result of NAD depletion. Within the glutaminase domain, from our modelling, Cys49 resides close to Tyr51 which forms a hydrophobic component of the first major bottleneck of the ammonia channel, and interacts with the highly conserved YRE loop.[19] Mutation of Tyr51 results in reduced stability of the protein.[16] The p.Cys49Arg mutation might result in loss of a disulfide bond to Cys53, thereby maligning the interaction of Tyr51 with the YRE loop and similarly destabilizing the glutaminase domain. Trp132 likely forms a cation-π interaction with Lys114 which forms part of the catalytic triad[23] that stabilizes the glutaminase active site. Corresponding p.Lys114Ala mutations in yeast and bacteria lack glutaminase activity and are inviable *in vivo*,[22; 24] suggesting that p.Trp132Leu mutation might mimic this loss of interaction and destabilize the glutaminase domain. Our studies show that the p.Trp132Leu mutant exhibits ~81-fold decreased NAD synthetase-specific activity compared to WT NADSYN1 (Figure 3C) and, while the p.Cys49Arg mutant could not be similarly assessed enzymatically, its reduced expression and stability suggest a deleterious impact on NADSYN1 activity. Together, both missense variants contribute to the NAD deficit in individual F3.II.4.

In postnatal tissue, *Nadsyn1* is highly expressed in the small intestine, kidney, liver, and testis while weakly expressed in the heart and skeletal muscle.[15] This parallels enzymatic activity *in vivo* with kidney and liver exhibiting the highest NADSYN1 activity, and to a lesser extent the small intestine, heart, and spleen.[4] However, it is currently unclear how NAD deficiency disrupts embryonic development. In mice, NAD deficiency causes the same complex abnormalities[5] as seen here in individuals with *NADSYN1* mutation. Moreover, in mice, disrupted development is apparent at embryonic day 9.5 (H.C., unpublished data; equivalent to human day 22), a stage that includes tissue induction and patterning, and progenitor cell development and deployment, both key to organogenesis. It will be important to determine which of the NAD-dependent processes (metabolism, ATP production, biosynthesis, DNA repair and stress responses) are individually or collectively responsible for the observed disruption of embryogenesis.

NADSYN1, like many non-redundant genes of the *de novo* NAD synthesis pathway from tryptophan (Table S2), appears tolerant to heterozygous missense mutation (0.91 observed/expected missense variants) in humans.[10] This is, however, expected of genes causing recessive disease, as a single deleterious allele may be compensated for by the other allele.[25] Nevertheless, here we expand the genotypic spectrum of Congenital NAD Deficiency Disorder to that of biallelic missense variants, and expect individuals harboring biallelic variants in additional genes of this pathway (*AFMID, KMO*, and *QPRT*) to be similarly susceptible to NAD deficiency and congenital malformation. Through a combination of yeast complementation assays, observation of altered mutant protein levels, and enzymatic analysis of mammalian-expressed NADSYN1 protein, we show that disease-causal variants impair catalytic activity of the enzyme, resulting in impaired NAD synthesis. We further recommend that biallelic loss-of-function variants in the *NADSYN1* gene be recognized as a cause of Congenital NAD Deficiency Disorder, and that additional nonredundant genes of this pathway be considered in unresolved cases characterized by defects in the vertebrae, heart, and kidney such as VACTERL association.[26] Furthermore, it is conceivable that defects induced by genetic insult of *NADSYN1* may be rescued via NAD precursor-rich dietary supplementation, as has been demonstrated for *Haao*- or *Kynu*-deficient mice.[5]

Supplemental Data

Supplemental Data include three figures and two tables.

Acknowledgements

The authors would like to thank the families for their participation in the study. The authors acknowledge the technical assistance of Joelene Greasby, Kathryn Hill, and Antony Cooper, and Ignatia Van Den Veyver for providing clinical information. This work was supported by National Health and Medical Research Council (NHMRC) [Project Grant ID 1162878 to S.L.D and G.C, and Fellowship ID1135886 to S.L.D]; Office of Health and Medical Research NSW Government to S.L.D.; The Key Foundation to S.L.D.; Canadian Institutes of Health Research (MOP133593) to T.A.D.; Children's Health Research Institute TRGF to T.A.D. and V.S.

Declaration of Interests

Baylor College of Medicine (BCM) and Miraca Holdings Inc. have formed a joint venture with shared ownership and governance of Baylor Genetics (BG), formerly Baylor Miraca Genetics Laboratories, which performs chromosomal microarray analysis and clinical exome sequencing. During preparation of this manuscript, R.X. was an employee of BCM and derived support through a professional services agreement with BG. The remaining authors declare that they have no competing interests.

Web Resources

CADD score, https://cadd.gs.washington.edu/score
ClinVar, https://www.ncbi.nlm.nih.gov/clinvar/
GnomAD, https://gnomad.broadinstitute.org/gene/ENSG00000172890
OMIM, https://omim.org/

Accession Numbers

The *NADSYN1* variants reported in this manuscript are accessible in ClinVar with the submission number SUB6305474.

References

1. Kirkland, J.B. (2012). Niacin requirements for genomic stability. Mutat Res 733, 14-20.
2. Rajman, L., Chwalek, K., and Sinclair, D.A. (2018). Therapeutic Potential of NAD-Boosting Molecules: The In Vivo Evidence. Cell Metab 27, 529-547.
3. Nikiforov, A., Kulikova, V., and Ziegler, M. (2015). The human NAD metabolome: Functions, metabolism and compartmentalization. Crit Rev Biochem Mol Biol 50, 284-297.
4. Mori, V., Amici, A., Mazzola, F., Di Stefano, M., Conforti, L., Magni, G., Ruggieri, S., Raffaelli, N., and Orsomando, G. (2014). Metabolic profiling of alternative NAD biosynthetic routes in mouse tissues. PLoS One 9, e113939.
5. Shi, H., Enriquez, A., Rapadas, M., Martin, E., Wang, R., Moreau, J., Lim, C.K., Szot, J.O., Ip, E., Hughes, J.N., et al. (2017). NAD Deficiency, Congenital Malformations, and Niacin Supplementation. N Engl J Med 377, 544-552.
6. Sobreira, N., Schiettecatte, F., Valle, D., and Hamosh, A. (2015). GeneMatcher: a matching tool for connecting investigators with an interest in the same gene. Hum Mutat 36, 928-930.
7. Rentzsch, P., Witten, D., Cooper, G.M., Shendure, J., and Kircher, M. (2018). CADD: predicting the deleteriousness of variants throughout the human genome. Nucleic Acids Res, gky1016-gky1016.
8. Adzhubei, I., Jordan, D.M., and Sunyaev, S.R. (2013). Predicting functional effect of human missense mutations using PolyPhen-2. Curr Protoc Hum Genet Chapter 7, Unit7 20.
9. Davydov, E.V., Goode, D.L., Sirota, M., Cooper, G.M., Sidow, A., and Batzoglou, S. (2010). Identifying a high fraction of the human genome to be under selective constraint using GERP++. PLoS Comput Biol 6, e1001025.
10. Karczewski, K.J., Francioli, L.C., Tiao, G., Cummings, B.B., Alföldi, J., Wang, Q., Collins, R.L., Laricchia, K.M., Ganna, A., Birnbaum, D.P., et al. (2019). Variation across 141,456 human exomes and genomes reveals the spectrum of loss-of-function intolerance across human protein-coding genes. bioRxiv, 531210.
11. Suda, Y., Tachikawa, H., Yokota, A., Nakanishi, H., Yamashita, N., Miura, Y., and Takahashi, N. (2003). Saccharomyces cerevisiae QNS1 codes for NAD(+) synthetase that is functionally conserved in mammals. Yeast 20, 995-1005.
12. Bieganowski, P., and Brenner, C. (2004). Discoveries of nicotinamide riboside as a nutrient and conserved NRK genes establish a Preiss-Handler independent route to NAD(+) in fungi and humans. Cell 117, 495-502.
13. Giaever, G., and Nislow, C. (2014). The yeast deletion collection: a decade of functional genomics. Genetics 197, 451-465.
14. Graeff, R., and Lee, H.C. (2002). A novel cycling assay for cellular cADP-ribose with nanomolar sensitivity. Biochem J 361, 379-384.
15. Hara, N., Yamada, K., Terashima, M., Osago, H., Shimoyama, M., and Tsuchiya, M. (2003). Molecular identification of human glutamine- and ammonia-

dependent NAD synthetases. Carbon-nitrogen hydrolase domain confers glutamine dependency. J Biol Chem 278, 10914-10921.
16. Chuenchor, W., Doukov, T.I., Resto, M., Chang, A., and Gerratana, B. (2012). Regulation of the intersubunit ammonia tunnel in Mycobacterium tuberculosis glutamine-dependent NAD+ synthetase. Biochem J 443, 417-426.
17. Devedjiev, Y., Symersky, J., Singh, R., Jedrzejas, M., Brouillette, C., Brouillette, W., Muccio, D., Chattopadhyay, D., and DeLucas, L. (2001). Stabilization of active-site loops in NH3-dependent NAD+ synthetase from Bacillus subtilis. Acta Crystallogr D Biol Crystallogr 57, 806-812.
18. Jauch, R., Humm, A., Huber, R., and Wahl, M.C. (2005). Structures of Escherichia coli NAD synthetase with substrates and products reveal mechanistic rearrangements. J Biol Chem 280, 15131-15140.
19. LaRonde-LeBlanc, N., Resto, M., and Gerratana, B. (2009). Regulation of active site coupling in glutamine-dependent NAD(+) synthetase. Nat Struct Mol Biol 16, 421-429.
20. De Ingeniis, J., Kazanov, M.D., Shatalin, K., Gelfand, M.S., Osterman, A.L., and Sorci, L. (2012). Glutamine versus ammonia utilization in the NAD synthetase family. PLoS One 7, e39115.
21. Wojcik, M., Seidle, H.F., Bieganowski, P., and Brenner, C. (2006). Glutamine-dependent NAD+ synthetase. How a two-domain, three-substrate enzyme avoids waste. J Biol Chem 281, 33395-33402.
22. Bieganowski, P., Pace, H.C., and Brenner, C. (2003). Eukaryotic NAD+ synthetase Qns1 contains an essential, obligate intramolecular thiol glutamine amidotransferase domain related to nitrilase. J Biol Chem 278, 33049-33055.
23. Pace, H.C., Hodawadekar, S.C., Draganescu, A., Huang, J., Bieganowski, P., Pekarsky, Y., Croce, C.M., and Brenner, C. (2000). Crystal structure of the worm NitFhit Rosetta Stone protein reveals a Nit tetramer binding two Fhit dimers. Curr Biol 10, 907-917.
24. Bellinzoni, M., Buroni, S., Pasca, M.R., Guglierame, P., Arcesi, F., De Rossi, E., and Riccardi, G. (2005). Glutamine amidotransferase activity of NAD+ synthetase from Mycobacterium tuberculosis depends on an amino-terminal nitrilase domain. Res Microbiol 156, 173-177.
25. Roca, I., Fernandez-Marmiesse, A., Gouveia, S., Segovia, M., and Couce, M.L. (2018). Prioritization of Variants Detected by Next Generation Sequencing According to the Mutation Tolerance and Mutational Architecture of the Corresponding Genes. Int J Mol Sci 19, 1584.
26. Stevenson, R.E., and Hunter, A.G. (2013). Considering the Embryopathogenesis of VACTERL Association. Molecular syndromology 4, 7-15.
27. Adzhubei, I.A., Schmidt, S., Peshkin, L., Ramensky, V.E., Gerasimova, A., Bork, P., Kondrashov, A.S., and Sunyaev, S.R. (2010). A method and server for predicting damaging missense mutations. Nat Methods 7, 248-249.

Figure Titles and Legends

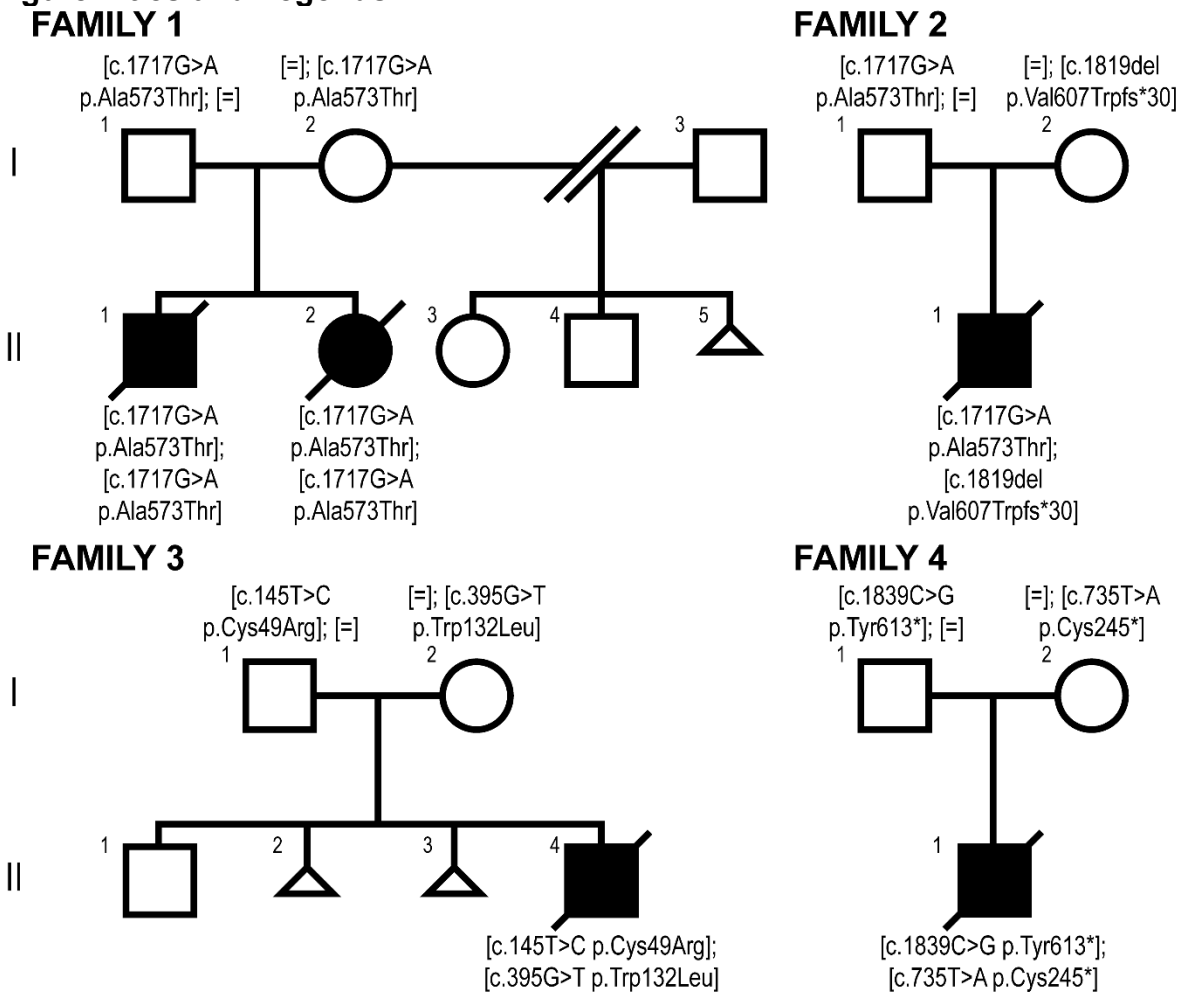

Figure 1. Pedigrees of four unrelated families harboring pathogenic biallelic *NADSYN1* mutations in individuals with Congenital NAD Deficiency Disorder. Phenotypes of affected individuals are presented in Table 1 and the Supplemental Note. In Family 3, II.2 was a blighted ovum, while II.3 was a first trimester miscarriage.

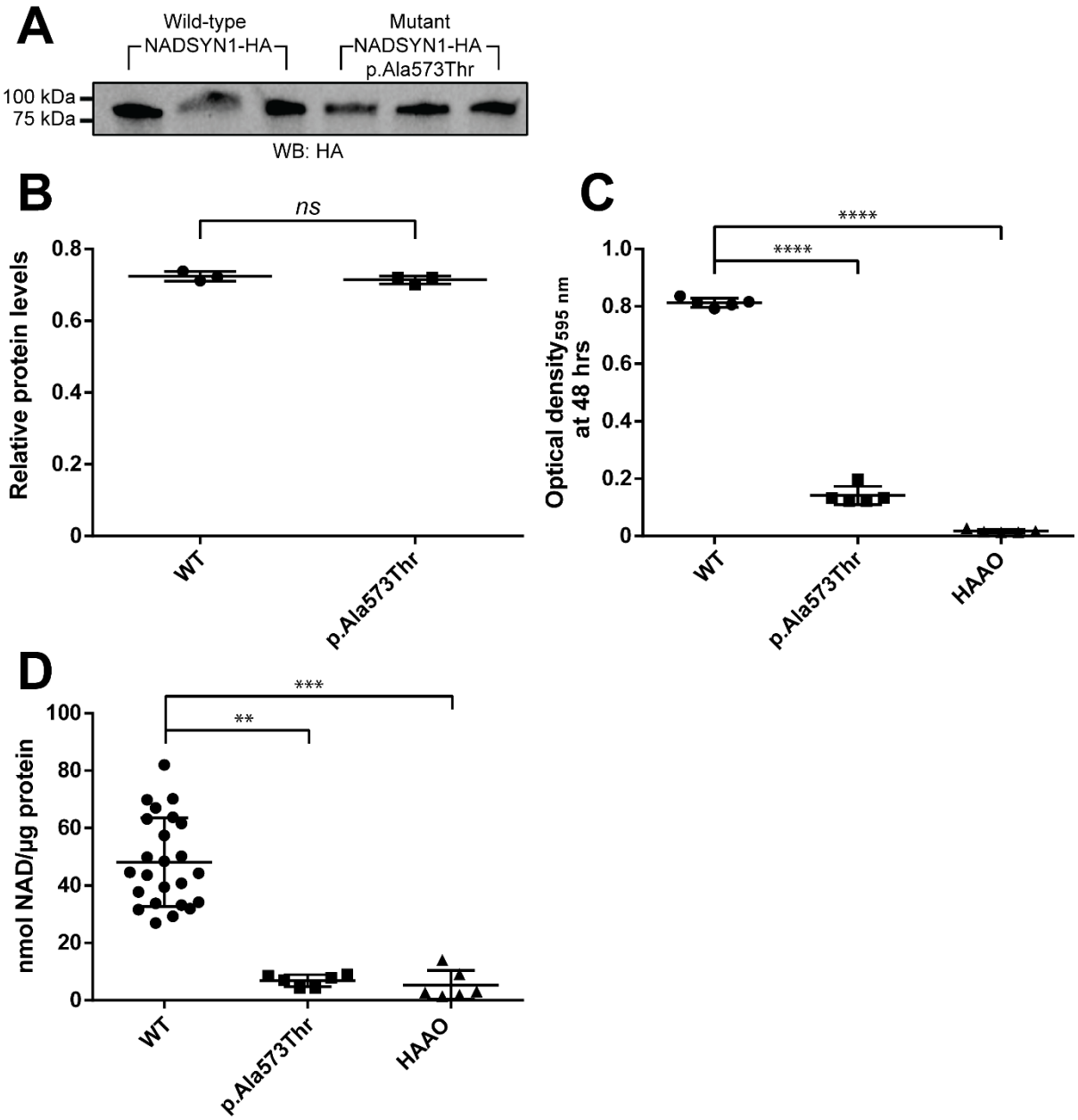

Figure 2. Genetic complementation of yeast Qns1p with human NADSYN1. (A) Protein lysates from Δ*qns1* yeast generating wild-type (WT) NADSYN1-HA (Δ*qns1* WT) or p.Ala573Thr (Δ*qns1* p.Ala573Thr) mutant, grown in nicotinamide riboside (NR)-supplemented conditions in triplicate, detected with an anti-HA antibody; WB: western blot; (B) Quantification of detected protein, normalized to total lane protein; (C) Δ*qns1* WT, p.Ala573Thr mutant, or HAAO control yeast, seeded at $OD_{595\ nm}$ 0.01, were grown in the absence of NR with $OD_{595\ nm}$ measurements taken at 48 hrs. **** $p < 0.0001$, one-way ANOVA with Tukey's multiple comparisons test, horizontal bars indicate mean and standard deviation; (D) NAD^+/H concentrations in yeast cultures grown for 48 hrs with NR, then without NR for 8 hrs, normalized to protein lysate. ** $p = 0.0012$, *** $p = 0.0002$, horizontal bars indicate mean and standard deviation, Kruskal-Wallis with Dunn's multiple corrections test.

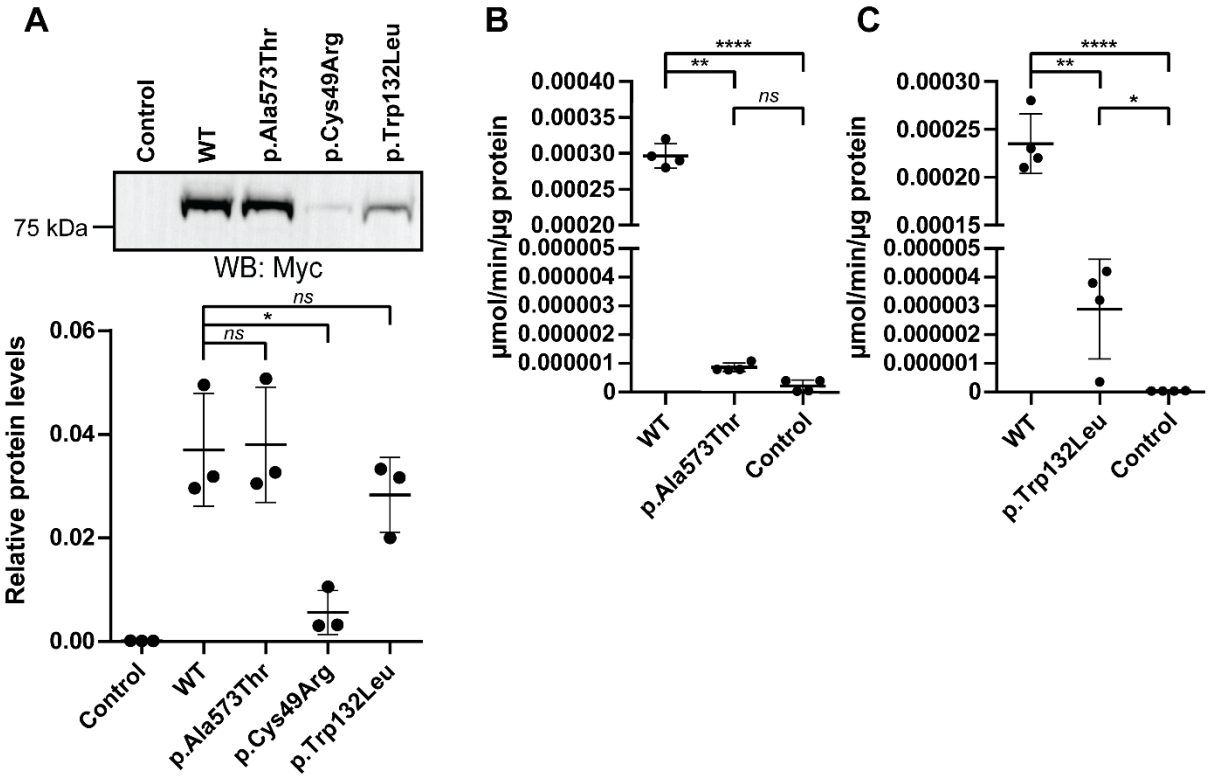

Figure 3. Functional assessment of mammalian-expressed human NADSYN1 protein compared to pathogenic missense variants identified in affected individuals. (A) Mammalian-expressed human NADSYN1 and mutant protein lysates and their levels relative to total lane protein, detected with an anti-Myc antibody, * p = 0.0417, ns = not significant; WB: western blot, horizontal bars indicate mean and standard deviation, Brown-Forsythe and Welch one-way ANOVA; (B) NAD synthetase activity of purified p.Ala573Thr mutant compared to wild-type (WT) NADSYN1 protein, ** p = 0.0026, **** p <0.0001; ns = not significant, horizontal bars indicate mean and standard deviation, Brown-Forsythe and Welch one-way ANOVA; (C) Enzymatic activity of purified p.Trp132Leu mutant compared to WT NADSYN1 protein; * p = 0.0167, ** p = 0.0096, **** p <0.0001, horizontal bars indicate mean and standard deviation, Brown-Forsythe and Welch one-way ANOVA.

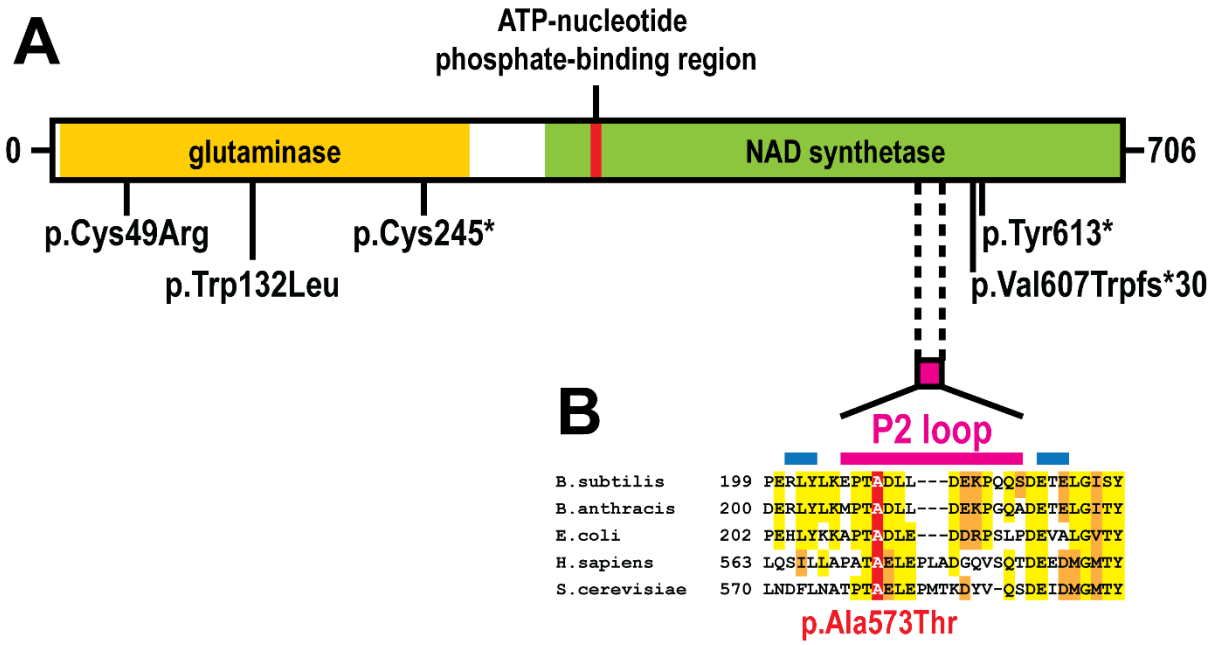

Figure 4. Protein domain diagram of human NADSYN1 highlighting the position of mutations identified in individuals. (A) Positions of missense and frameshift variants relative to protein domains identified in affected individuals. (B) Position of the p.Ala573Thr variant (red) relative to an evolutionarily conserved region defined as the P2 loop (pink), alpha helices (blue). ClustalW sequence alignment adapted from Jauch et al. [18]

Tables

Table 1. Clinical summary of individuals with *NADSYN1* mutations

Family	Individual [variant]	Gender	Gestation at birth	Birth Weight (g)	Vertebral	Cardiac	Renal	Limb	Other
Family 1	II.1 [c.1717G>A p.Ala573Thr]; [c.1717G>A p.Ala573Thr]	Male	38 w 2 d	2665	Thoracic vertebral defect	Hypoplastic mitral valve with borderline hypoplastic left ventricle, small bicuspid aortic valve and tubular hyperplasia of the left aortic arch with coarctation, anomalous origin of the left coronary artery from the right pulmonary artery	Absent left kidney	Bilateral shortening of humeri and femora	Sacral dimple
	II.2 [c.1717G>A p.Ala573Thr]; [c.1717G>A p.Ala573Thr]	Female	23 w 4 d	410	Multiple segmentation and formation defects of the thoracic, lumbar, and sacral spine [a]	Absent left ventricle and pulmonary trunk, right ventricular outlet to the aorta	Bilateral hypoplastic kidneys	Short humeri and femora	nil

Family 2	II.1 [c.1717G>A p.Ala573Thr]; [c.1819del p.Val607Trpfs*30]	Male	39 w 5 d	3380	Scoliosis with multiple malformed vertebral anomalies and rib abnormalities	DORV, TGA in side by side orientation, doubly committed VSD, bidirectional PDA, left aortic arch	Mild hyperechoic renal cortex	Birth length: 45.5 cm, short proximal long bones, bowing of lower extremities	Closed sacral dimple with tuft of hair
Family 3	II.4 [c.145T>C p.Cys49Arg]; [c.395G>T p.Trp132Leu]	Male	TOP 16 w	na	na	na	Oligohydramnios, bilateral renal agenesis	na	na
Family 4	II.1 [c.735T>A p.Cys245*]; [c.1839C>G p.Tyr613*]	Male	TOP 16 w	na	na	na	Left renal and ureter agenesis	Micromelia, bilateral club feet	Hydrocephalus, small thorax, echogenic bowel, flat nose and low set ears, oedema, polysplenia, pulmonary hypoplasia

[a] See Figure S2; d: days; DORV: double outlet right ventricle; PDA: patent ductus arteriosus; na: not assessed; nil: no abnormality detected; TGA: transposition of the great arteries; TOP: termination of pregnancy; w: weeks; VSD: ventricular septal defect

Table 2. *NADSYN1* variants identified in affected individuals and their predicted pathogenicity

Individual	cDNA change	Protein change	PolyPhen-2 HVAR[27]	CADD-PHRED[7]	GERP++[9]	Population frequency (with respect to gnomAD[10])
F1.II.1, F1.II.2, F2.II.1	1717G>A	Ala573Thr	1	24.3	4.83	7.40E-04
F2.II.1	1819del	Val607Trpfs*30	na	23	na	7.07E-06
F3.II.4	145T>C	Cys49Arg	0.553	33	5.63	7.97E-06
F3.II.4	395G>T	Trp132Leu	0.989	24.5	4.95	4.65E-04
F4.II.1	735T>A	Cys245*	na	35	na	Novel
F4.II.1	1839C>G	Tyr613*	na	41	na	Novel

PolyPhen-2 HVAR: Score ≥0.909: probably damaging; 0.908 ≤ score ≤ 0.447: possibly damaging; score ≤0.446: benign; CADD-PHRED: scaled CADD score ≥15: damaging; GERP++, >2: evolutionarily constrained; na: not applicable

Supplemental Data

Supplemental Note: Case Reports.

Individual F1.II.1

A male infant was born at 38 weeks 2 days, weighing 2665 g (3rd percentile) to a healthy 32 year old GTPAL42012 woman after antenatal diagnosis of hypoplastic left heart syndrome with shortened humeri and femora. Postnatal cardiac findings included hypoplastic mitral valve with borderline hypoplastic left ventricle, small bicuspid aortic valve, and tubular hypoplasia of the left aortic arch with coarctation. At 5 days of life, he underwent a hybrid stage 1 procedure with insertion of bilateral pulmonary artery bands and patent ductus arteriosus stent. He died unexpectedly on day of life 32. At autopsy, he was non-dysmorphic with weight 3231 g, length 47.5 cm, and head circumference 32.5 cm, all at the third percentile. Cardiac pathology revealed circumferential subendocardial left ventricular infarction with previously undetected anomalous origin of the left coronary artery from the right pulmonary artery. There was unilateral left renal agenesis, testes were descended, brain was small at 370 g (460 ± 47 g). Note was made of a sacral dimple. Family history was positive for a half first cousin (mother's maternal half-sister's son) with coarctation of the aorta, ventricular septal defect and bicuspid aortic valve, as well as a more distant cousin (mother's maternal aunt's son) with transposition of the great arteries.

Individual F1.II.2

In the subsequent pregnancy, a female sibling to Individual F1.II.1 was delivered at 23 weeks and 4 days gestation after antenatal ultrasound revealed multiple foetal anomalies, including a hypoplastic left heart, shortened humeri and femora, a left-sided choroid plexus cyst, an irregular appearance to the foetal distal spine, and possible ambiguous genitalia. Chromosomal microarray performed on cells obtained at amniocentesis was reported as an apparently normal female, with no genomic imbalance. Early induction occurred at 23 weeks 4 days gestation. Autopsy revealed a small non-dysmorphic infant weighing 410 g (3rd percentile) with head circumference of 19.5 cm (10th percentile). Complex cardiac malformation consisted of normal superior and inferior vena cava attachments to a normal right atrium, draining into a single right ventricle with outlet to the aorta. Pulmonary trunk was absent and the pulmonary veins drained into the left atrium. Mitral orifice and mitral valve were absent. Kidneys were hypoplastic with a combined weight of 2.6 g (5.3 ± 1.8 g). The brain weighed 58.3 g (74 ± 11 g) with normal structure. External genitalia were normal female. Skeletal survey demonstrated relatively short humeri and femora with multiple segmentation and formation defects of the thoracic, lumbar, and sacral spine (Figure S2). The appendicular skeleton, ribs, and skull were unremarkable.

Individual F2.II.1

A male infant was born at 39 weeks 5 days, weighing 3380 g to a healthy 18-year old G1P0 woman. Apgar scores were 4 at 1 min, 7 at 5 mins. He was flaccid with poor respiratory effort. Complex congenital heart defects were appreciated on prenatal echocardiogram. Postnatal ECHO showed double outlet right ventricle with transposed great arteries in side-by-side orientation, doubly committed and

unrestrictive ventricular septal defect. The left ventricle is borderline size. Mitral valve annulus is small. Patent foramen ovale is left-to-right shunting. Patent ductus arteriosus is large and bidirectional shunting. No Doppler evidence of coarctation of the aortic arch. Twelve-lead electrocardiogram showed sinus tachycardia and right ventricular hypertrophy with repolarization abnormalities. Physical examination identified short proximal long bones, bowing of the lower extremities, short thorax, closed sacral dimple with tuft of hair, and scoliosis with multiple malformed vertebral and rib anomalies. Ophthalmologic exam was normal without colobomas. Renal ultrasound showed a hyperechoic renal cortex relative to liver with no discrete cystic dysplasia and slightly heterogeneous pericalyceal and peripelvic echoes of uncertain significance. Abdominal ultrasound shows likely pyloric stenosis. Chromosomal microarray was normal and chromosomal breakage analysis was negative. The following variants of unknown significance, additional to *NADSYN1*, were identified in individual F2.II.1: NM_198428.3(*BBS9*):c.214del p.Val72Trpfs*12 (paternally inherited), NM_024582.4(*FAT4*):c.11372T>C p.Leu3791Pro (paternally inherited) and c.3658T>A p.Ser1220Thr (maternally inherited), NM_024408.4(*NOTCH2*):c.646C>G p.Gln216Glu) (paternally inherited), NM_015335.4(*MED13L*):c.5413A>G p.Ile805Val (paternally inherited), NM_001369.2(*DNAH5*):c.8018A>G p.Asn2673Ser, and NM_003777.3(*DNAH11*):c.8798-5G>T. None of these variants were considered disease-causal.

Individual F3.II.4

The fourth pregnancy of a healthy 37-year old G4P1031 woman presented with oligohydramnios at 15 weeks of gestation. She denied any significant exposure to alcohol, tobacco, drugs, or other known teratogens during pregnancy. Ultrasound at 16 weeks was unable to locate evidence of renal tissue and the pregnancy was terminated due to lethal anomaly. Foetal autopsy was performed and confirmed a male foetus with bilateral renal agenesis, and a small tubular bladder due to lack of urine production. No other anomalies or dysmorphism was noted. The couple's first pregnancy resulted in a healthy currently 5 year old boy, while second and third pregnancies resulted in a first trimester miscarriage (Figure 1, F3.II.2) and blighted ovum (Figure 1, F3.II.3), respectively. Both couple's family histories were reported to be negative for known birth defects or intellectual disabilities. The foetus was negative for *CHD7* mutation, while karyotype (46, XX) and microarray analysis revealed no abnormalities. Individual F3.II.4 had no alternative reportable variants.

Individual F4.II.1

This is the first pregnancy of a healthy 29-year old woman. Dating scan was performed at 6 weeks of gestation to confirm the gestational age. Nuchal translucency was 4.3 mm at 12 weeks. Severe oligohydramnios was detected on ultrasound at 16 weeks. In addition, bilateral hydrocephalus and micromelia were noted. The right kidney could be seen while left kidney was not clear on ultrasound, possibly due to an unfavourable foetal position. Bilateral club feet and echogenic bowels were also noted. The chest was relatively small compared with the abdomen. The medical termination and postmortem were performed at 16 weeks. Potter syndrome was suspected. Additional features include left renal and ureter agenesis, right kidney obstructive dysplasia due to abnormal ureter, flattened nose and low set ears, oedema, polysplenia, and probable pulmonary hypoplasia. Adrenals were on both sides and nodular kidney on right with dilated but distally atretic ureter, but

nothing on the left side. Non-invasive prenatal testing was normal for individual F4.II.1. The following variants of unknown significance, additional to *NADSYN1*, were identified in individual F4.II.1: NM_001377.3(*DYNC2H1*):c.2703-7T>A (maternally inherited) and NM_001377.3(*DYNC2H1*):c.1385G>A p.Arg462Gln (paternally inherited). None of these variants were considered disease-causal.

Supplemental Figures

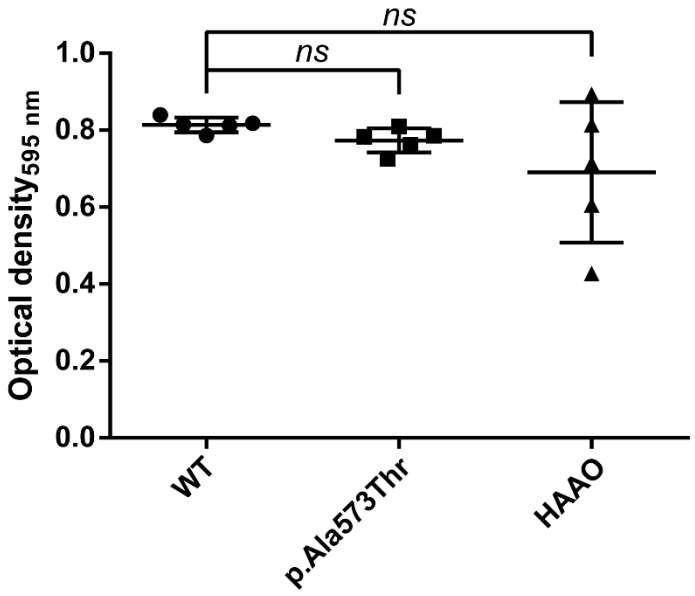

Figure S1. Δ*qns1* yeast growth in the presence of nicotinamide riboside is independent of NADSYN1 or HAAO synthesis. Δ*qns1* yeast generating wild-type (WT) NADSYN1-HA, p.Ala573Thr mutant, or HAAO control, seeded at $OD_{595\ nm}$ 0.01, were grown in the presence of nicotinamide riboside with $OD_{595\ nm}$ measurements taken at 48 hrs. ns: not significant.

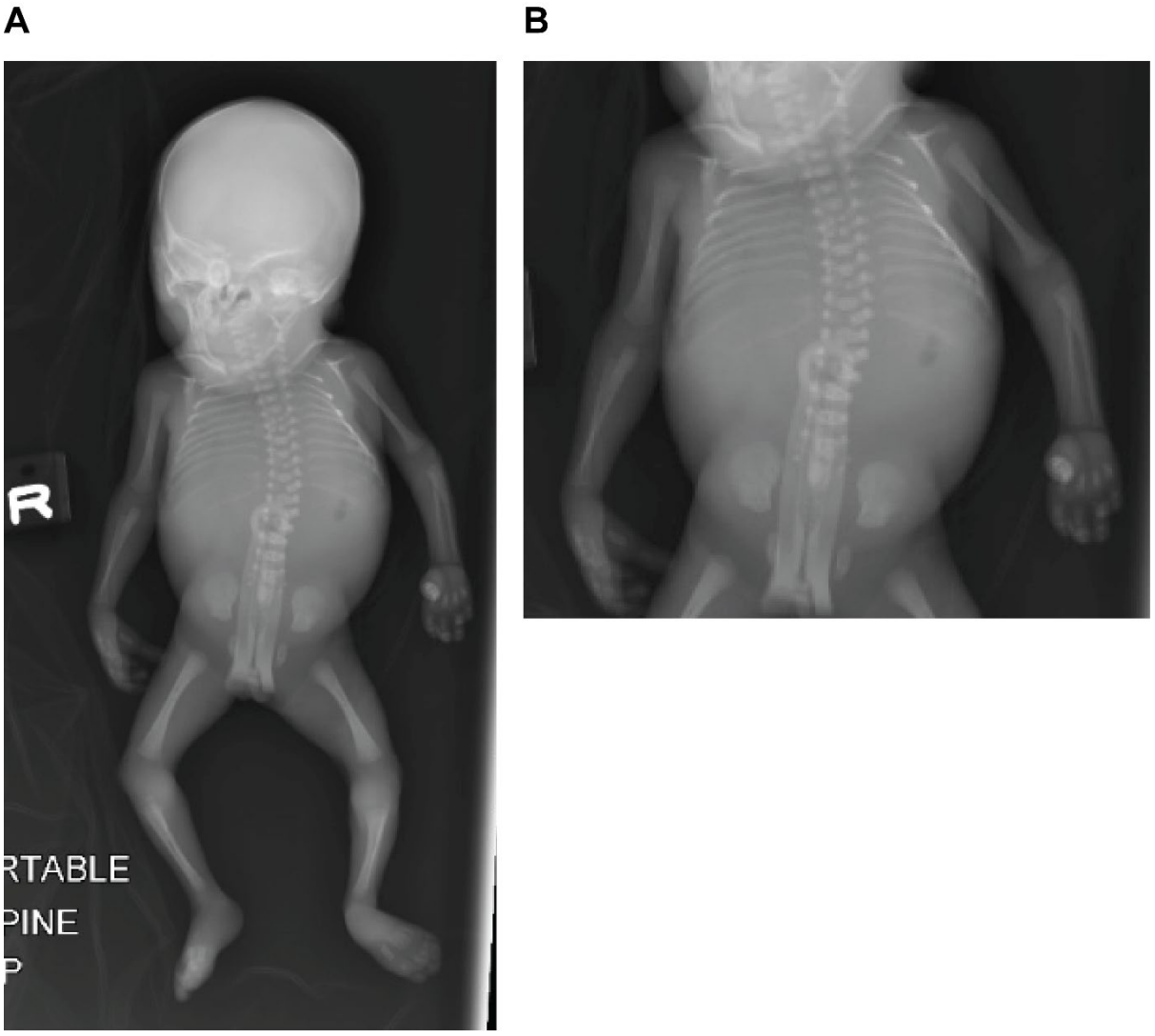

Figure S2. X-rays of individual F1.II.2. (A) Relative short humeri and femora; (B) multiple segmentation and fusion defects of the thoracic, lumbar, and sacral spine.

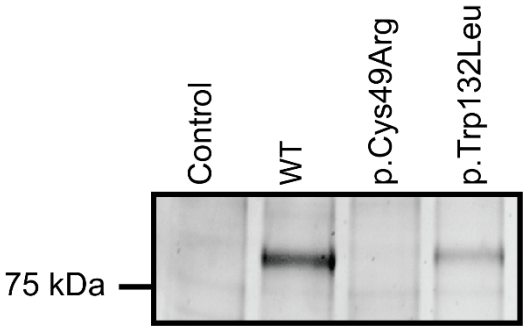

Figure S3. Coomassie-stained gel of purified wild-type and mutant NADSYN1 protein used for enzymatic assessment. Equal amounts of NADSYN1 proteins purified from transiently transfected COS-7 cells. Control represents purification of protein lysate from untransfected cells.

Supplemental Tables

Table S1: Phenotypic comparison of *de novo* NAD gene pathway variants identified to date

Gene	Individual [variant]	Gender	Gestation at birth	Birth Weight (g)	Vertebral	Cardiac	Renal	Limb	Other
NADSYN1[a]	F1.II.1 [c.1717G>A p.Ala573Thr]; [c.1717G>A p.Ala573Thr]	Male	38 w 2 d	2665	Thoracic vertebral defect	Hypoplastic mitral valve with borderline hypoplastic left ventricle, small bicuspid aortic valve and tubular hypoplasia of the left aortic arch with coarctation, anomalous origin of the left coronary artery from the right pulmonary artery	Absent left kidney	Bilateral shortening of humeri and femora	Sacral dimple
	F1.II.2 [c.1717G>A p.Ala573Thr]; [c.1717G>A p.Ala573Thr]	Female	23 w 4 d	410	Multiple segmentation and formation defects of the thoracic, lumbar, and sacral spine	Absent left ventricle and pulmonary trunk, right ventricular outlet to the aorta	Bilateral hypoplastic kidneys	Bilateral shortening of humeri and femora	nil
	F2.II.1 [c.1717G>A p.Ala573Thr]; [c.1819del p.Val607Trpfs*30]	Male	39 w 5 d	3380	Scoliosis with multiple malformed vertebral anomalies and rib abnormalities	Double outlet right ventricle, transposition of the great arteries in side by side orientation, doubly committed ventricular septal defect, bidirectional patent ductus arteriosus, left aortic arch	Mild hyperechoic renal cortex	Birth length: 45.5 cm, short proximal long bones, bowing of lower extremities	Closed sacral dimple with tuft of hair
	F3.II.4 [c.145T>C p.Cys49Arg]; [c.395G>T p.Trp132Leu]	Male	TOP 16 w	na	na	na	Oligohydramnios, bilateral renal agenesis	na	na
	F4.II.1 [c.735T>A p.Cys245*]; [c.1839C>G p.Tyr613*]	Male	TOP 16 w	na	na	na	Left renal and ureter agenesis	Micromelia, bilateral club feet	Hydrocephalus, small thorax, echogenic bowel, flat nose and low set ears, oedema, polysplenia, pulmonary hypoplasia
HAAO[b]	A [c.483dupT p.Asp162*]; [c.483dupT p.Asp162*]	Male	34	2240	Spinal lipoma, sacral agenesis, thoracic and lumbar segmentation defects	Atrial septal defect	Hypoplastic right kidney	Talipes	Short stature, global developmental delay, intellectual disability, laryngeal web, laryngomalacia
	B [c.588G>A p.Trp186*]; [c.588G>A p.Trp186*]	Female	38	2680	Thoracic and lumbar segmentation defects	Hypoplastic left heart	Hypoplastic kidney	nil	Palsy of left vocal chord
KYNU[b]	C [c.170-1G>T p.Val57Glufs*21]; [c.170-1G>T p.Val57Glufs*21]	Female	39	3715	Thoracic segmentation defects	Patent ductus arteriosus	Hypoplastic kidney	Talipes, syndactyly, rhizomelia	Anterior anus
	D [c.468T>A p.Tyr156*]; [c.1045_1051delTTTAAGC p.Phe349Lysfs*4]	Female	38	2460	Segmentation defects	Hypoplastic left heart	Solitary left kidney, moderate chronic kidney disease	Shortened long bones	Short stature, speech delay

[a]From this study; [b]from Shi et al. [1]; d: days; na: not assessed; nil: no abnormality detected; TOP: termination of pregnancy; w: weeks

Table S2. Tolerance of nonredundant *de novo* NAD synthesis pathway genes to mutation

				Observed/expected (heterozygous)[a]			
Gene	Name	HGNC ID	MIM# (if available)	Missense	Loss-of-function	pLI	Number of tolerated homozygous frameshifts[a]
AFMID	arylformamidase	20910	-	0.974	0.724	0	0
KMO	kynurenine 3-monooxygenase	6381	-	0.683	0.431	0	0
HAAO	3-hydroxyanthranilate 3,4-dioxygenase	4796	617660	1.039	0.741	0	0
KYNU	kynureninase	6469	617661	1.074	0.891	0	0
QPRT	quinolinate phosphoribosyltransferase	9755	-	0.772	0.522	0	0
NADSYN1	NAD synthetase 1	29832	-	0.906	0.699	0	0

[a] With respect with gnomAD[2]; HGNC: HUGO Gene Nomenclature Committee; MIM: Mendelian Inheritance in Man; pLI: probability of being loss-of-function intolerant

Supplemental Methods

Whole exome sequencing and genetic analyses

Individuals F1.II.1 and F1.II.2

Using genomic DNA from the proband and parents, the exonic regions and flanking splice junctions of the genome were captured using the IDT xGen Exome Research Panel v1.0. Massively parallel (NextGen) sequencing was done on an Illumina system with 100 bp or greater paired-end reads. Reads were aligned to human genome build GRCh37/UCSC hg19 and analyzed for sequence variants using a custom-developed analysis tool. Additional sequencing technology and variant interpretation protocol has been previously described.[3]

Variant segregation analysis was subsequently performed on the affected siblings and their parents. 98.3% of coding exons and splice junctions of protein-coding RefSeq genes that are captured by massively parallel (NextGen) sequencing had at least 10× coverage with a mean depth of coverage at 72×. A homozygous variant in *NADSYN1* (NM_018161.5) c.1717G>A p.Ala573Thr was identified in both affected children, inherited from heterozygous parents (Figure 1), and was considered a variant of uncertain significance. No additional *de novo*, compound heterozygous, homozygous, heterozygous, or X-linked variants were considered pathogenic or contributory to the individuals' phenotypes. In view of the individuals' phenotypes, analysis specifically included review of genes associated with hypoplastic left heart, complete absence of the left ventricle, small cerebellum, skeletal abnormalities, short femur, short humerus, vertebral defects, hypoplastic kidneys, and VACTERL association.

Individuals F2.II.1, F3.II.4, and F4.II.1

Clinical exome sequencing and analysis was performed as previously reported[4; 5], identifying biallelic mutations in *NADSYN1*.

Cloning of yeast expression constructs

Human NADSYN1 was PCR amplified from pOTB7 NADSYN1 (MGC:4508) with primers *EcoRI-5-NADSYN1* and *3-NADSYN1-HA-EcoRI*. This was subsequently inserted into pEntr2B (Thermo Fischer) via ligation of *EcoRI*-cut vector and insert. Via Gateway LR reaction, NADSYN1 was introduced into pAG416GPD (a gift from A. Ayer, VCCRI, NSW, Australia; Addgene plasmid #14148) from pEntr2B NADSYN1-HA, generating pAG416GPD NADSYN1-HA.

The c.1717A>G p.Ala573Thr variant was introduced into pOTB7 NADSYN1 cDNA by site-directed mutagenesis with primers *NADSYN1 A573Tmut F* and *NADSYN1 A573Tmut R* using the KAPA HiFi kit according to manufacturer's instructions. An internal fragment cut with *BglII* and *NdeI* surrounding the Ala573Thr variant was inserted into pEntr2B NADSYN1-HA. The resultant NADSYN1-HA Ala573Thr insert was introduced into yeast expression vector pAG416GPD as described above. Plasmids were verified for correct sequence identity by Sanger sequencing. Human *HAAO* cDNA was amplified from MHC:BC029510 using primers *HAAO for* and *HAAO rev*, then gateway cloned into pDONR201 via BP reaction (Thermo Fisher) according to manufacturer's instructions. Finally, the *HAAO* insert was transferred to pAG416GPD by Gateway LR reaction as described above.

Name	Primer sequence	Purpose
EcoRI-5-NADSYN1	tatagaattcaaaaaaatgggccggaaggtgaccgt	Amplifying *NADSYN1* from pOTB7 with *EcoRI* ends
3-NADSYN1-EcoRI	tatagaattcaaaaaaatgggccggaaggtgaccgt	Amplifying *NADSYN1* from pOTB7 with *EcoRI* ends
3-NADSYN1-HA-EcoRI	tatagaattcttaagcgtaatctggaacatcgtatgggtagtccacgccgtccaggg	Amplifying *NADSYN1* from pOTB7 with *EcoRI* ends (C-terminal -HA tagged alternate)
NADSYN1 A573Tmut F	gcgccggccaccacggagctggagccc	Forward mutagenesis primer introducing A573T into human *NADSYN1* cDNA
NADSYN1 A573Tmut R	gggctccagctccgtggtggccggcgc	Reverse mutagenesis primer introducing A573T into human *NADSYN1* cDNA
kanMX4 DNstream45	ctcgtggaaagtcttattttgctgtgagcacttcttctgtgcta	kanMX4 with homology arms amplification (2nd round)
kanMX4 UPstream45	ccccaaataccctggcattctttttttgactccctgccagtaatg	kanMX4 with homology arms amplification (2nd round)
kanMX4 DNTAG	agcacttcttctgtgctacggtgtcggtctcgtagtgctcaacacctggcaattaatccgatgaattcgagctcg	kanMX4 with homology arms amplification (1st round)
kanMX4 UPTAG	gactccctgccagtaatggatgtccacgaggtctcttaatgcactataagcaccgccgtacgctgcaggtcgac	kanMX4 with homology arms amplification (1st round)
HAAO for	ggggacaagtttgtacaaaaaagcaggcttcaccatggagcgccgcctg	*HAAO* cDNA amplification with BP overhangs
HAAO rev	ggggaccactttgtacaagaaagctgggtctcaccccaggggcttcttg	*HAAO* cDNA amplification with BP overhangs
Nadsyn1 forward	ggggacaagtttgtacaaaaaagcaggctccaccatgggccggaaggtgacc	Amplifying *NADSYN1* with mammalian Kozak sequence from pAG416GPD NADSYN1
Nadsyn1 reverse	gggaccactttgtacaagaaagctgggtcgtccacgccgtccaggga	Amplifying *NADSYN1* with mammalian Kozak sequence from pAG416GPD NADSYN1
C49R forward	tggaccagactggaaatacgcggctacgg	Forward mutagenesis primer introducing C49R into human *NADSYN1* cDNA
C49R reverse	ccgtagccgcgtatttccagctctggtcca	Reverse mutagenesis primer introducing C49R into human *NADSYN1* cDNA
W132L forward	tggttcaccccgttgtcgaggagtcgg	Forward mutagenesis primer introducing W132L into human *NADSYN1* cDNA
W132L reverse	ccgactcctcgacaacggggtgaacca	Reverse mutagenesis primer introducing W132L into human *NADSYN1* cDNA

Yeast BY4742 *qns1Δ::kanMX4* generation and transformations

QNS1, yeast homolog of human *NADSYN1*, was replaced with a *kanMX4* cassette by homologous recombination as previously described[6] with the following modifications: pFA6-kanMX4 (a gift from A. Cooper, Garvan Institute of Medical Research, NSW, Australia) was PCR amplified with UPTAG and DNTAG primers, followed by a second PCR amplification with UPstream45 and DNstream45 primers, transformed into haploid *Saccharomyces cerevisiae* BY4742 (*MATα hisΔ1 leu2Δ0 lys2Δ0 ura3Δ0*; a gift from A. Cooper, Garvan Institute of Medical Research, NSW, Australia) using the Yeast Transformation Kit (Sigma) according to manufacturer's instructions. Transformed yeast were transferred onto agar plates (20 g/L Agar bacteriological (Agar No. 1; Oxoid), 20 g/L D-(+)-glucose (Sigma), 1.7 g/L Yeast Nitrogen Base, without amino acids, without ammonium sulfate (AMRESCO); 5 g/L ammonium sulfate (Sigma), 20.4 mg/L Nicotinamide riboside chloride (NR) (MedKoo Biosciences), amino acids (Sigma): 260 mg/L leucine, 180 mg/L lysine, 76 mg/L isoleucine, 120 mg/L valine, 46 mg/L histidine, 90 mg/L tryptophan, 55 mg/L adenine). Positive transformants were restreaked onto YAPD plates (20 g Agar bacteriological (Agar No. 1; Oxoid); 20 g/L Bacteriological peptone (Oxoid); 20 g/L D-(+)-glucose (Sigma); 10 g/L Bacto™ Yeast extract (BD Biosciences); 40 mg/L adenine hemisulfate salt (Sigma)) with G418 selection (320 mg/L, Geneticin; Invivogen). BY4742 Δ*qns1::kanMX4* was confirmed by genotyping with primers *qns1-Aconfirm*, *qns1-Bconfirm*, *qns1-Cconfirm*, *qns1-Dconfirm*, *KanB*, and *KanC*.

Δ*qns1* yeast were then transformed with pAG416GPD NADSYN1-HA, pAG416GPD NADSYN1-HA Ala573Thr, or pAG416GPD HAAO using the Yeast Transformation Kit (Sigma) according to manufacturer's instructions, plated as described above. *HAAO* encodes for the human homolog of yeast *BNA1*, upstream of *NADSYN1*/*QNS1* in the NAD biosynthesis pathway from tryptophan and is not expected to functionally compensate for the absence of Qns1p. Positive transformants were subsequently genotyped for correct plasmid insertion via direct PCR from yeast cultures[7] and Sanger sequencing.

Yeast lysate immunoblot

Δ*qns1* yeast generating WT NADSYN1-HA (Δ*qns1* WT) or p.Ala573Thr mutant were grown for 48 hrs in minimal media (6.71 g/L YNB+Nitrogen-Niacin powder, Sunrise Science Products; 1.92 g/L Yeast Synthetic Drop-Out Medium Supplements (-uracil); 20 g/L D-(+)-glucose (Sigma)) supplemented with 20.4 mg/L NR at 30°C. Cells were subsequently lysed and protein extracted as previously described.[8] 50 µg of protein was loaded on a 4-15% GTX Stain-Free acrylamide gels (Biorad) in denaturing conditions with SeeBlue Plus2 prestained protein ladder (Biorad). The Stain-Free gel was activated using the Chemidoc Stain-Free gel activation protocol. The proteins were transferred to a nicrocellulose membrane (0.45 µm pore size, Amersham). Transference of protein was confirmed by imaging the membrane using the Stain-Free blot protocol of the Chemidoc. Rabbit anti-HA antibody (C29F4, 1:1000, Cell Signalling Technologies) was used to detect HA-tagged NADSYN1 protein using WesternBreeze (Thermofisher Scientific) according to the manufacturer's instructions. Quantification of band intensity was performed using ImageJ. Statistical comparisons of band intensity normalized to total lane protein were made with GraphPad Prism software using a Mann-Whitney U test.

Yeast Growth Assays

Δ*qns1* WT, p.Ala573Thr mutant, or HAAO yeast were grown in a shaker at 30°C for 48 hrs in minimal media supplemented with 20.4 mg/L NR, washed in minimal media, then resuspended at an optical density ($OD_{595\ nm}$) of 0.05, and grown for a further 48 hrs in triplicate in minimal media ± NR. $OD_{595\ nm}$ measurements were taken at regular intervals throughout this time, ending at 48 hrs. Minimal media (-NR) was made identically to growth media (+NR) with the exception of NR. Statistical comparisons of $OD_{595\ nm}$ at 48 hrs were made with GraphPad Prism software using a one-way ANOVA with Tukey's multiple comparisons test.

Enzymatic NAD^+/NADH assays

Δ*qns1* WT, p.Ala573Thr, or HAAO yeast were grown in a shaker at 30°C for 48 hrs in minimal media supplemented with 20.4 mg/L nicotinamide riboside chloride. Yeast were washed, resuspended in minimal media lacking NR, and grown for a further 8 hrs. Cell pellets were ground under mortar and pestle in a liquid N_2-cooled environment, lysed in 0.2 M NaOH, 0.5% CTAB and 1/5 cell volume acid-washed beads (212-300 µm, Sigma) by vortexing. After centrifugation, supernatant was neutralised in equal parts with 0.5 M TRIS-HCl pH 6.8. Finally, lysates were assessed for total NAD via an enzymatic cycling reaction in which diaphorase catalyses the conversion of resazurin to the fluorescent resorufin, as previously described.[9] Reaction mix was made in water containing 100 mM TRIS-HCl pH 8, 5% ethanol, 0.5 mg/mL bovine serum albumin, 0.5% NP-40, 10 µM riboflavin mononucleotide, 15 U/mL alcohol dehydrogenase, 0.56 U/mL diaphorase, and 32 µM resazurin. $Excitation_{540nm}$/$emission_{590nm}$ measurements were taken every 2 min for 12 mins, using a FLUOstar OPTIMA Microplate Reader (BMG Labtech, Ortenberg, Germany), and compared to NAD standards made through serial dilution at known concentrations. Enzymatic activity was assessed in duplicate and normalised to total protein concentrations, assessed by Pierce BCA Protein assay (Thermo Fisher Scientific) according to manufacturer's instructions. Statistical comparisons of total NAD normalized to total protein concentration were made with GraphPad Prism software using a Kruskal-Wallis with Dunn's multiple corrections test.

Mammalian NADSYN1 expression and purification

Cloning of human expression constructs

Human WT NADSYN1 and NADSYN1 harbouring the Ala573Thr mutation was PCR amplified from pAG416GPD NADSYN1 and pAG416GPD NADSYN1 Ala573Thr, respectively, with NADSYN1 mutagenesis primers. The purified PCR products were BP cloned into pDONR201 using the Gateway System (BP Clonase enzyme mix, Thermo Fisher). Subsequently, pcDNA3.1 NADSYN1 myc-His (and pcDNA3.1 NADSYN1 Ala573Thr myc-His) was created by Gateway LR cloning (Gateway LR Clonase, Invitrogen) pDONR201 NADSYN1 and pDONR201 NADSYN1 Ala573Thr into pcDNA3.1 GW myc-His. NADSYN1 Cys49arg and Trp132Leu expression constructs were generated by mutagenesis of WT NADSYN1 pcDNA3.1 myc-His using primers listed above.

Mammalian expression and protein purification

COS-7 cells were grown to 70-80% confluency on 3×10 cm dishes. Cells were transfected with either pcDNA3.1 NADSYN1 myc-His, pcDNA3.1 NADSYN1 Ala573Thr myc-His, or pcDNA3.1 NADSYN1 Trp132Leu myc-His using Lipofectamine LTX reagent (Lipofectamine LTX with Plus Reagent, Thermo Fisher). The transfection mix was aspirated after 8 hrs and replaced with normal growth media (DMEM high glucose +10% FBS). 48 hrs post-transfection, NADSYN1 was purified using HisPur Ni-NTA magnetic beads as per manufacturer's instructions (HisPur Ni-NTA Magnetic beads, Thermo Fisher). For protein purification, all washes and all buffers including equilibration, wash, and elution buffers, were made up in 1× PBS (0.0027 M KCl, 0.137 M NaCl pH 7.4). Beads were incubated with sonicated protein extract for 1 hr on an end-over-end rotor. Eluted proteins were quantified using a Nanodrop (Thermo Fisher) and Pierce BCA protein assay kit (Thermo Scientific). In addition, 2 µL of purified protein was run on a 4-12% Bis-Tris protein gel (NuPAGE, Invitrogen) with BSA standards ranging from 25-200 ng. The gel was stained overnight with InstantBlue Coomasie protein stain (Expedeon) and rinsed several times with Milli-Q water. The de-stained gel was scanned using ChemiDoc Imaging system (Bio-Rad) and the bands were quantified using Image lab analysis software (Bio-Rad).

Mammalian protein lysate immunoblot

COS-7 cells were grown to 70-80% confluency on 3×10 cm dishes. Cells were transfected with either pcDNA3.1 NADSYN1 myc-His, pcDNA3.1 NADSYN1 Ala573Thr myc-His, pcDNA3.1 NADSYN1 Cys49Arg myc-His or pcDNA3.1 NADSYN1 Trp132Leu myc-His using Lipofectamine LTX reagent (Lipofectamine LTX with Plus Reagent, Thermo Fisher). The transfection mix was aspirated after 8 hrs and replaced with normal growth media (DMEM high glucose +10%FBS). 24 hrs post-transfection, cells were scrapped in PBS and lysed with 60 µL Whole-Cell Extract (WCE) buffer (20 mM HEPES pH7.8, 0.42M NaCl, 0.5% NP40, 25% Glycerol, 0.2 mM EDTA, 1.5 mM MgCl2, 1mM PMSF) containing protease inhibitors (cOmplete, mini protease inhibitor cocktail, Roche). 50 µg of protein was loaded on 4-15% MiniProtean TGX Stain-Free gels (Biorad) in denaturing conditions with Precision Plus protein standard (Biorad). The Stain-Free gel was activated using the Chemidoc Stain-Free gel activation protocol. The proteins were transferred to a PVDF membrane (0.45 µm pore size, Merck). WT NADSYN1 and mutants were detected with anti-Myc antibody (clone: 9E10). Quantification of band intensity was performed using Image Lab (BioRad). Statistical comparisons of band intensity normalized to total lane protein were made with GraphPad Prism software using a Brown-Forsythe and Welch one-way ANOVA test.

Enzymatic assays of mammalian-expressed NADSYN1

Enzyme assays were adapted from Hara et al.[10] Briefly, a reaction mix (20 µL) was made using 50 mM Tris-Cl^- (pH 7.5), 56 mM KCl, 5 mM $MgCl_2$, 10 µg BSA, 2 mM ATP, 2 mM dithiothreitol, 20 mM L-Glutamine, and 1 mM NaAD. Per 20 µL of reaction mix, 0.2 µg of protein was added and NAD^+/NADH enzyme assay was performed for 0-240 mins at 37°C. At each 30 min timepoint, reactions were terminated by addition of 112 µL 10 M NaOH and kept on ice. After completion of all timepoints, reactions were incubated at 37°C for 30 mins. Fluorescence intensity

was measured at 350 nm and 460 nm using a PHERAstar (BMG Lab Tech). The amount of NAD^+/NADH was calculated using known NAD concentrations used as standards. Statistical comparisons of enzymatic activity were made with GraphPad Prism software using a Brown-Forsythe and Welch one-way ANOVA test.

Supplemental References

1. Shi, H., Enriquez, A., Rapadas, M., Martin, E., Wang, R., Moreau, J., Lim, C.K., Szot, J.O., Ip, E., Hughes, J.N., et al. (2017). NAD Deficiency, Congenital Malformations, and Niacin Supplementation. N Engl J Med 377, 544-552.
2. Lek, M., Karczewski, K.J., Minikel, E.V., Samocha, K.E., Banks, E., Fennell, T., O'Donnell-Luria, A.H., Ware, J.S., Hill, A.J., Cummings, B.B., et al. (2016). Analysis of protein-coding genetic variation in 60,706 humans. Nature 536, 285-291.
3. Retterer, K., Juusola, J., Cho, M.T., Vitazka, P., Millan, F., Gibellini, F., Vertino-Bell, A., Smaoui, N., Neidich, J., Monaghan, K.G., et al. (2016). Clinical application of whole-exome sequencing across clinical indications. Genet Med 18, 696-704.
4. Yang, Y., Muzny, D.M., Xia, F., Niu, Z., Person, R., Ding, Y., Ward, P., Braxton, A., Wang, M., Buhay, C., et al. (2014). Molecular findings among patients referred for clinical whole-exome sequencing. JAMA 312, 1870-1879.
5. Yang, Y., Muzny, D.M., Reid, J.G., Bainbridge, M.N., Willis, A., Ward, P.A., Braxton, A., Beuten, J., Xia, F., Niu, Z., et al. (2013). Clinical whole-exome sequencing for the diagnosis of mendelian disorders. N Engl J Med 369, 1502-1511.
6. Giaever, G., and Nislow, C. (2014). The yeast deletion collection: a decade of functional genomics. Genetics 197, 451-465.
7. Amberg, D.C., Burke, D.J., and Strathern, J.N. (2006). Yeast colony PCR. CSH Protoc 2006, prot4170.
8. Dunn, B., and Wobbe, C.R. (1992). Preparation of Protein Extracts from Yeast. In Curr Protoc Mol Biol. (John Wiley & Sons, Inc.), pp 13.13.11-13.13.19.
9. Graeff, R., and Lee, H.C. (2002). A novel cycling assay for cellular cADP-ribose with nanomolar sensitivity. Biochem J 361, 379-384.
10. Hara, N., Yamada, K., Terashima, M., Osago, H., Shimoyama, M., and Tsuchiya, M. (2003). Molecular identification of human glutamine- and ammonia-dependent NAD synthetases. Carbon-nitrogen hydrolase domain confers glutamine dependency. J Biol Chem 278, 10914-10921.